Frontiers of Information Technology & Electronic Engineering
www.jzus.zju.edu.cn; engineering.cae.cn; www.springerlink.com
ISSN 2095-9184 (print); ISSN 2095-9230 (online)
E-mail: jzus@zju.edu.cn

Consensus-based three-dimensional multi-UAV formation control strategy with high precision*

Mao-de YAN[1], Xu ZHU‡[1], Xun-xun ZHANG[1], Yao-hong QU[2]

([1]*School of Electronic and Control Engineering, Chang'an University, Xi'an 710064, China*)

([2]*School of Automation, Northwestern Polytechnical University, Xi'an 710129, China*)

E-mail: mdyan@chd.edu.cn; zhuxu_1987@sina.com; zhangxunxun0427@163.com; qyh0809@nwpu.edu.cn

Received Jan. 4, 2016; Revision accepted Apr. 12, 2016; Crosschecked June 20, 2017

Abstract: We propose a formation control strategy for multiple unmanned aerial vehicles (multi-UAV) based on second-order consensus, by introducing position and velocity coordination variables through neighbor-to-neighbor interaction to generate steering commands. A cooperative guidance algorithm and a cooperative control algorithm are proposed together to maintain a specified geometric configuration, managing the position and attitude respectively. With the whole system composed of the six-degree-of-freedom UAV model, the cooperative guidance algorithm, and the cooperative control algorithm, the formation control strategy is a closed-loop one and with full states. The cooperative guidance law is a second-order consensus algorithm, providing the desired acceleration, pitch rate, and heading rate. Longitudinal and lateral motions are jointly considered, and the cooperative control law is designed by deducing state equations. Closed-loop stability of the formation is analyzed, and a necessary and sufficient condition is provided. Measurement errors in position data are suppressed by synchronization technology to improve the control precision. In the simulation, three-dimensional formation flight demonstrates the feasibility and effectiveness of the formation control strategy.

Key words: Multiple unmanned aerial vehicles; Consensus; Cooperative guidance; Cooperative control; Synchronization technology

http://dx.doi.org/10.1631/FITEE.1600004 **CLC number:** TP391

1 Introduction

Recently, the formation control of multiple unmanned aerial vehicles (multi-UAV) has been an active topic (Shan and Liu, 2005; Jing and Shi, 2014) since it promises many practical applications, such as reconnaissance, surveillance, atmospheric study, communication relaying, and search and rescue. Multi-UAV formation has the unique advantage over a single UAV in that it has higher efficiency and less fuel consumption. In other words, multi-UAV formation control has good prospects in both military and civil fields.

Some research methods have been proposed for multi-UAV control, such as leader-follower (Mercado *et al.*, 2013), behavior-based approach (Kim and Kim, 2007), virtual structure (Ren and Beard, 2002), and artificial potential function (Bennet *et al.*, 2011). These methods have different advantages, but the communication topology between UAVs is rarely considered, so they cannot make full use of information flow and sharing. To use the information flow to improve synchronization of the entire formation, the consensus method has attracted more and more interest of researchers (Kumar *et al.*, 2005;

‡ Corresponding author

* Project supported by the National Natural Science Foundation of China (No. 61473229), the Special Fund for Basic Scientific Research of Central Colleges, Chang'an University, China (Nos. 310832163403 and 310832161012), the Key Science and Technology Program of Shaanxi Province, China (No. 2017JQ6060), and the Xi'an Science and Technology Plan, China (No. CXY1512-3)

ORCID: Xu ZHU, http://orcid.org/0000-0002-3616-4336

Kuriki and Namerikawa, 2013). The consensus algorithms require only neighbor-to-neighbor interaction and carry out a decentralized control strategy, which minimizes power consumption, increases stealth, and improves the scalability of the formation (Kuriki and Namerikawa, 2014).

Consensus can make the formation evolve as a rigid body in a given direction with some given orientation and maintain the geometric relationship. For more specific formation flight problems of UAVs, the consensus is that the vehicles should be able to achieve tracking for the given velocity, heading, and altitude commands (Kumar *et al.*, 2005). Some effort of consensus has been devoted to multi-UAV formation control. A consensus-based feedback linearization method has been proposed to maintain a specified time-varying geometric configuration for formation flight (Seo *et al.*, 2009). The formation guidance problem can also be solved by consensus theory (Chen and Zhang, 2013). For collision-avoidance of multiple UAVs, a consensus strategy coupled with artificial potential function has been proposed (Kuriki and Namerikawa, 2014). A testbed was even constructed to validate the consensus algorithm, using a global positioning system (Aldo *et al.*, 2010).

However, most of the existing literature on consensus recognizes the UAV as a point mass (Wang *et al.*, 2010; Li *et al.*, 2012). Some scholars assumed that an automatic pilot operates in the inner loop and its executive capability is infinite (Bai *et al.*, 2009). Both the above assumptions are too idealistic to be used in practice. Moreover, the relationship between cooperative guidance and cooperative control is seldom studied.

Besides, to decrease the influence of disturbances and measurement errors, some methods have been found and adopted, such as proportional-integral-derivative (PID) control (Xiao *et al.*, 2011), H_∞ control (Wang *et al.*, 2012), sliding mode control (Hou *et al.*, 2011), and model predictive control (Annamalai *et al.*, 2015). Unfortunately, PID control cannot suppress nonlinear disturbances, and H_∞ control is conservative in finding a weight function. Though the common sliding-mode controller is easily designed and invariant with the change of system parameters and disturbances, the oscillation caused by discontinuous control restricts its application. Model predictive control has shown better performance than the traditional linear quadratic Gaussian (LQG). Hence, it is expected that higher control accuracy of the formation can be acquired through an effective and efficient way to reduce disturbances and measurement errors.

Therefore, it is of great need to solve these critical problems and advance consensus in application. In this study, we focus on formation control using consensus with high precision. Compared to Fukushima *et al.* (2013), instead of generating a number of subproblems and solving optimization problems, our formation control strategy involves less computational burden. Compared to Ren (2006), our formation control strategy is closed-loop and with full states, as the whole system consists of the six-degree-of-freedom UAV model as well as the cooperative guidance and cooperative control algorithms. A cooperative guidance algorithm and a cooperative control algorithm are proposed and united. To clearly demonstrate the relationship between cooperative guidance and cooperative control, the coordination variable is used as the key connection point, and cooperative control is treated as the inner loop of cooperative guidance. To improve the control accuracy of the formation, measurement errors in sensor data are reduced by synchronization technology.

2 Problem formulation and background

Consider a formation of n identical UAVs, each denoted by U_i ($i \in \{1, 2, \ldots, n\}$). They constitute a directed graph $\mathcal{G} = \{\mathcal{V}, \mathcal{E}\}$, where $\mathcal{V} = \{U_1, U_2, \ldots, U_n\}$ is the set of nodes, and $\mathcal{E} \subseteq \mathcal{V} \times \mathcal{V}$ is the set of edges in which an edge of the graph $\mathcal{G}$ is denoted by e_{ij}. Note that e_{ij} is a directed edge from U_j to U_i such that U_i can obtain information composed of position and velocity from U_j. The set of neighbors for U_i is denoted by $\mathcal{N}_i = \{U_j \in \mathcal{V} : e_{ij} \in \mathcal{E}\}$. Define a non-negative adjacency weight a_{ij} associated with the edge e_{ij}. Moreover, assume that $a_{ii} = 0$ for all $U_i \in \mathcal{V}$.

After describing the communication topology, choosing the coordination variables becomes another major issue of consensus, as consistent coordination variables are the final objective. Position and velocity coordination variables are selected such that velocity V_i can be used as velocity coordination variables directly, whereas the choice of the position

coordination variables is more complicated.

For this purpose, the definition of the position coordination variable will be given. It is defined as a reference point $\boldsymbol{\rho}_{i\mathrm{F}}$, and the position vector from U_i to its reference point is denoted by $\boldsymbol{\rho}_{i\mathrm{F}}^{\mathrm{d}}$. The geometric configuration and position coordination variables are demonstrated in Fig. 1 in both the unsteady case and the steady case.

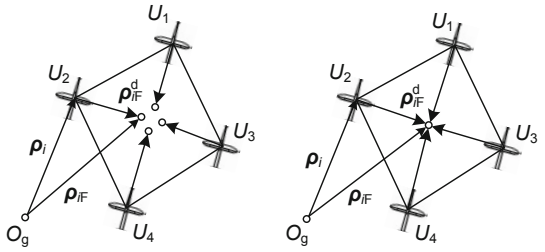

Fig. 1 Position coordination variable $\boldsymbol{\rho_{i\mathrm{F}}}$: (a) unsteady case; (b) steady case

Suppose that the predefined geometric configuration of the formation is known. The position coordination variable is obtained by vector computation:

$$\boldsymbol{\rho}_{i\mathrm{F}} = \boldsymbol{\rho}_i + \boldsymbol{\rho}_{i\mathrm{F}}^{\mathrm{d}}. \tag{1}$$

If $\boldsymbol{\rho}_{i\mathrm{F}} \to \boldsymbol{\rho}_{j\mathrm{F}}$ as $t \to \infty$, the formation is achieved as in Fig. 1b.

3 Multi-UAV formation control

A multi-UAV formation control system consists of a cooperative guidance system and a cooperative control system. The cooperative control system aims to control the attitude in the inner loop, and the cooperative guidance system is used to control the position in the outer loop, where the output of the outer loop is used as the input of the inner loop. As measurement errors and synchronization errors can significantly degrade the system performance, synchronization technology is used to suppress these errors and improve the control accuracy of the multi-UAV formation system. The structure of the multi-UAV formation control is depicted in Fig. 2.

3.1 Cooperative guidance

A second-order consensus algorithm is adopted to design the cooperative guidance system. Longitudinal, lateral, and altitudinal channels are designed,

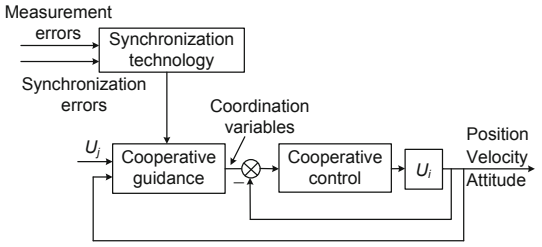

Fig. 2 Structure of the multi-UAV formation control

respectively, as follows:

$$\begin{cases} \dot{V}_{x_i}^{\mathrm{g}} = -\sum\limits_{j\in\mathcal{N}_i} a_{ij}[x_{i\mathrm{F}} - x_{j\mathrm{F}} - \gamma\dot{x}_{ij}], \\ \dot{V}_{y_i}^{\mathrm{g}} = -\sum\limits_{j\in\mathcal{N}_i} a_{ij}[y_{i\mathrm{F}} - y_{j\mathrm{F}} - \gamma\dot{y}_{ij}], \\ \dot{V}_{z_i}^{\mathrm{g}} = -\sum\limits_{j\in\mathcal{N}_i} a_{ij}[z_{i\mathrm{F}} - z_{j\mathrm{F}} - \gamma\dot{z}_{ij}], \end{cases} \tag{2}$$

where γ is a positive constant greater than 1 and $\dot{\boldsymbol{\rho}}_{ij} = (\dot{x}_{ij}, \dot{y}_{ij}, \dot{z}_{ij})^{\mathrm{T}}$ is the relative speed of U_j to U_i:

$$\begin{cases} \dot{x}_{ij} = \dot{x}_i - \dot{x}_j, \\ \dot{y}_{ij} = \dot{y}_i - \dot{y}_j, \\ \dot{z}_{ij} = \dot{z}_i - \dot{z}_j. \end{cases}$$

Though $\boldsymbol{\rho}_{i\mathrm{F}}$ is different from each other in the beginning, by controlling the three components of the acceleration given in Eq. (2) in the ground coordination system, the formation is stable if $\boldsymbol{\rho}_{i\mathrm{F}} \to \boldsymbol{\rho}_{j\mathrm{F}}$ as $t \to \infty$. Define the acceleration vector $\dot{\boldsymbol{V}}_i^{\mathrm{g}} = (\dot{V}_{x_i}^{\mathrm{g}}, \dot{V}_{y_i}^{\mathrm{g}}, \dot{V}_{z_i}^{\mathrm{g}})^{\mathrm{T}}$. To further design the formation-keeping algorithm based on consensus, $\dot{\boldsymbol{V}}_i^{\mathrm{g}}$ is transformed into a set of real guidance orders $\dot{V}_i^{\mathrm{g}}, \dot{\theta}_i^{\mathrm{g}}, \dot{\psi}_i^{\mathrm{g}}$, which are the desired acceleration, pitch rate, and heading rate, respectively:

$$\dot{V}_i^{\mathrm{g}} = \sqrt{\left(\dot{V}_{x_i}^{\mathrm{g}}\right)^2 + \left(\dot{V}_{y_i}^{\mathrm{g}}\right)^2 + \left(\dot{V}_{z_i}^{\mathrm{g}}\right)^2}, \tag{3}$$

$$\begin{aligned} \dot{\theta}_i^{\mathrm{g}} &= \frac{\mathrm{d}}{\mathrm{d}t}\left[\arctan\left(\frac{V_{z_i}^{\mathrm{g}}}{V_{x_i}^{\mathrm{g}}}\right)\right] \\ &= \frac{\dot{V}_{z_i}^{\mathrm{g}}\int_0^t \dot{V}_{x_i}^{\mathrm{g}}\mathrm{d}t - \dot{V}_{x_i}^{\mathrm{g}}\int_0^t \dot{V}_{z_i}^{\mathrm{g}}\mathrm{d}t}{\left(\int_0^t \dot{V}_{x_i}^{\mathrm{g}}\mathrm{d}t\right)^2 + \left(\int_0^t \dot{V}_{z_i}^{\mathrm{g}}\mathrm{d}t\right)^2}, \end{aligned} \tag{4}$$

$$\begin{aligned} \dot{\psi}_i^{\mathrm{g}} &= \frac{\mathrm{d}}{\mathrm{d}t}\left[\arctan\left(\frac{V_{y_i}^{\mathrm{g}}}{V_{x_i}^{\mathrm{g}}}\right)\right] \\ &= \frac{\dot{V}_{y_i}^{\mathrm{g}}\int_0^t \dot{V}_{x_i}^{\mathrm{g}}\mathrm{d}t - \dot{V}_{x_i}^{\mathrm{g}}\int_0^t \dot{V}_{y_i}^{\mathrm{g}}\mathrm{d}t}{\left(\int_0^t \dot{V}_{x_i}^{\mathrm{g}}\mathrm{d}t\right)^2 + \left(\int_0^t \dot{V}_{y_i}^{\mathrm{g}}\mathrm{d}t\right)^2}. \end{aligned} \tag{5}$$

For simplicity, define a new cooperative guidance law as follows:

$$\boldsymbol{v}_i = \left[\dot{V}_i^{\mathrm{g}}, \dot{\theta}_i^{\mathrm{g}}, \dot{\psi}_i^{\mathrm{g}}\right]^{\mathrm{T}}. \tag{6}$$

The formation can realize stability by Eq. (6) with the corresponding cooperative control system.

3.2 Cooperative control

A cooperative control law will be designed and divided into two channels, as the six-degree-of-freedom dynamics model of UAV is composed of longitudinal and lateral channels. Linear state equations for the longitudinal channel are given by

$$\begin{cases} \dot{\boldsymbol{x}}_i^{\text{long}} = \boldsymbol{A}^{\text{long}}\boldsymbol{x}_i^{\text{long}} + \boldsymbol{B}^{\text{long}}\boldsymbol{u}_i^{\text{long}}, \\ \boldsymbol{y}_i^{\text{long}} = \boldsymbol{C}^{\text{long}}\boldsymbol{x}_i^{\text{long}}, \end{cases} \tag{7}$$

where $\boldsymbol{x}_i^{\text{long}} = [V_i, \alpha_i, \theta_i, q_i, \delta_{\text{t}_i}, \delta_{\text{e}_i}]^{\text{T}}$ are the state variables, $\boldsymbol{u}_i^{\text{long}} = [\delta_{\text{t}_i,\text{d}}, \delta_{\text{e}_i,\text{d}}]^{\text{T}}$ are the inputs, and $\boldsymbol{y}_i^{\text{long}} = [V_i, \theta_i]^{\text{T}}$ are the outputs. Note that $\delta_{\text{t}_i}, \delta_{\text{e}_i}$ and $\delta_{\text{t}_i,\text{d}}, \delta_{\text{e}_i,\text{d}}$ represent the actual and desired thrust offsets and elevator deflections, respectively. The detailed form of $\dot{\boldsymbol{x}}_i^{\text{long}}$ is shown in Eq. (8) (in the next page), while the detailed form of $\boldsymbol{y}_i^{\text{long}}$ is as follows:

$$\begin{bmatrix} V_i \\ \theta_i \end{bmatrix} = \begin{bmatrix} 1 & 0 & 0 & 0 & 0 & 0 \\ 0 & 0 & 1 & 0 & 0 & 0 \end{bmatrix} \begin{bmatrix} V_i \\ \alpha_i \\ \theta_i \\ q_i \\ \delta_{\text{t}_i} \\ \delta_{\text{e}_i} \end{bmatrix}. \tag{9}$$

The linear state equations for the lateral channel are

$$\begin{cases} \dot{\boldsymbol{x}}_i^{\text{lat}} = \boldsymbol{A}^{\text{lat}}\boldsymbol{x}_i^{\text{lat}} + \boldsymbol{B}^{\text{lat}}\boldsymbol{u}_i^{\text{lat}}, \\ y_i^{\text{lat}} = \boldsymbol{C}^{\text{lat}}\boldsymbol{x}_i^{\text{lat}}, \end{cases} \tag{10}$$

where $\boldsymbol{x}_i^{\text{lat}} = [\beta_i, \phi_i, \psi_i, p_i, r_i, \delta_{\text{a}_i}, \delta_{\text{r}_i}]^{\text{T}}$ are the state variables, $\boldsymbol{u}_i^{\text{lat}} = [\delta_{\text{a}_i,\text{d}}, \delta_{\text{r}_i,\text{d}}]^{\text{T}}$ are the inputs, and $y_i^{\text{lat}} = \psi_i$ is the output. Note that $\delta_{\text{a}_i}, \delta_{\text{r}_i}$ and $\delta_{\text{a}_i,\text{d}}, \delta_{\text{r}_i,\text{d}}$ represent the actual and desired aileron and rudder deflections, respectively. The detailed form of $\dot{\boldsymbol{x}}_i^{\text{lat}}$ is shown in Eq. (11) (in the next page), while the detailed form of y_i^{lat} is as follows:

$$\psi_i = \begin{bmatrix} 0 & 0 & 1 & 0 & 0 & 0 & 0 \end{bmatrix} \begin{bmatrix} \beta_i \\ \phi_i \\ \psi_i \\ p_i \\ r_i \\ \delta_{\text{a}_i} \\ \delta_{\text{r}_i} \end{bmatrix}. \tag{12}$$

Then longitudinal and lateral equations can be expressed in a unified form as follows:

$$\begin{cases} \dot{\bar{\boldsymbol{x}}}_i = \bar{\boldsymbol{A}}\bar{\boldsymbol{x}}_i + \bar{\boldsymbol{B}}\boldsymbol{u}_i = \bar{\boldsymbol{A}} \begin{bmatrix} \boldsymbol{x}_i^{\text{long}} \\ \boldsymbol{x}_i^{\text{lat}} \end{bmatrix} + \bar{\boldsymbol{B}} \begin{bmatrix} \boldsymbol{u}_i^{\text{long}} \\ \boldsymbol{u}_i^{\text{lat}} \end{bmatrix}, \\ \bar{\boldsymbol{y}}_i = \bar{\boldsymbol{C}}\bar{\boldsymbol{x}}_i = \bar{\boldsymbol{C}} \begin{bmatrix} \boldsymbol{x}_i^{\text{long}} \\ \boldsymbol{x}_i^{\text{lat}} \end{bmatrix}, \end{cases} \tag{13}$$

where $\bar{\boldsymbol{A}} = \begin{bmatrix} \boldsymbol{A}^{\text{long}} & \boldsymbol{0} \\ \boldsymbol{0} & \boldsymbol{A}^{\text{lat}} \end{bmatrix}$, $\bar{\boldsymbol{B}} = \begin{bmatrix} \boldsymbol{B}^{\text{long}} & \boldsymbol{0} \\ \boldsymbol{0} & \boldsymbol{B}^{\text{lat}} \end{bmatrix}$, $\bar{\boldsymbol{C}} = \left[\boldsymbol{C}^{\text{long}},\ \boldsymbol{C}^{\text{lat}}\right]^{\text{T}}$, $\bar{\boldsymbol{x}}_i = \left[[\boldsymbol{x}_i^{\text{long}}]^{\text{T}},\ [\boldsymbol{x}_i^{\text{lat}}]^{\text{T}}\right]^{\text{T}}$ are the total state variables, input $\boldsymbol{u}_i$ are the four actuators, and $\bar{\boldsymbol{y}}_i = \left[[\boldsymbol{y}_i^{\text{long}}]^{\text{T}},\ y_i^{\text{lat}}\right]^{\text{T}}$ are the outputs.

Next, the cooperative control algorithm will be designed, whose structure is depicted in Fig. 3.

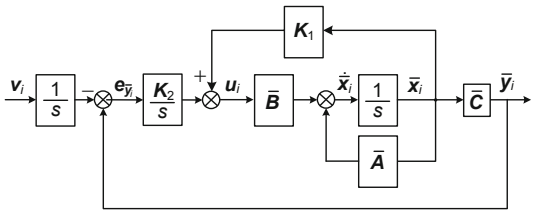

Fig. 3 Structure of the cooperative control algorithm

The control errors of $\bar{\boldsymbol{y}}_i$ are indicated as

$$\boldsymbol{e}_{\bar{\boldsymbol{y}}_i} = \bar{\boldsymbol{y}}_i - \int_0^t \boldsymbol{v}_i \mathrm{d}t. \tag{14}$$

Computing differentials of Eqs. (13) and (14), we obtain

$$\frac{\mathrm{d}}{\mathrm{d}t}\dot{\bar{\boldsymbol{x}}}_i = \bar{\boldsymbol{A}}\dot{\bar{\boldsymbol{x}}}_i + \bar{\boldsymbol{B}}\dot{\boldsymbol{u}}_i, \tag{15}$$

$$\frac{\mathrm{d}}{\mathrm{d}t}\boldsymbol{e}_{\bar{\boldsymbol{y}}_i} = \bar{\boldsymbol{C}}\dot{\bar{\boldsymbol{x}}}_i - \boldsymbol{v}_i. \tag{16}$$

It is easy to see that

$$\frac{\mathrm{d}}{\mathrm{d}t}\begin{bmatrix} \dot{\bar{\boldsymbol{x}}}_i \\ \boldsymbol{e}_{\bar{\boldsymbol{y}}_i} \end{bmatrix} = \begin{bmatrix} \bar{\boldsymbol{A}} & \boldsymbol{0} \\ \bar{\boldsymbol{C}} & \boldsymbol{0} \end{bmatrix} \begin{bmatrix} \dot{\bar{\boldsymbol{x}}}_i \\ \boldsymbol{e}_{\bar{\boldsymbol{y}}_i} \end{bmatrix} + \begin{bmatrix} \bar{\boldsymbol{B}} \\ \boldsymbol{0} \end{bmatrix} \dot{\boldsymbol{u}}_i + \begin{bmatrix} \boldsymbol{0} \\ -\boldsymbol{v}_i \end{bmatrix}. \tag{17}$$

If system (17) is controllable, it should satisfy

$$\operatorname{rank}\begin{bmatrix} \bar{\boldsymbol{A}} & \boldsymbol{0} \\ \bar{\boldsymbol{C}} & \boldsymbol{0} \end{bmatrix} = n_{\bar{\boldsymbol{A}}} + n_{\bar{\boldsymbol{C}}}, \tag{18}$$

where $n_{\bar{\boldsymbol{A}}}$ and $n_{\bar{\boldsymbol{C}}}$ are the ranks of matrices $\bar{\boldsymbol{A}}$ and $\bar{\boldsymbol{C}}$, respectively. The input for both longitudinal and lateral motions of the cooperative control law is

$$\boldsymbol{u}_i = \boldsymbol{K}_1\bar{\boldsymbol{x}}_i + \boldsymbol{K}_2\int_0^t \boldsymbol{e}_{\bar{\boldsymbol{y}}_i}\mathrm{d}t, \tag{19}$$

where $\boldsymbol{K}_1$ and $\boldsymbol{K}_2$ are feedback gains of the cooperative control law, selected using the pole placement method (Liu and Tang, 2000).

$$
\begin{bmatrix} \dot{V}_i \\ \dot{\alpha}_i \\ \dot{\theta}_i \\ \dot{q}_i \\ \dot{\delta}_{\mathrm{t}_i} \\ \dot{\delta}_{\mathrm{e}_i} \end{bmatrix} = \begin{bmatrix} X_V + X_{\mathrm{t}V}\cos\alpha_{\mathrm{e}} & X_{\mathrm{a}} & -g\cos\mu_{\mathrm{e}} & 0 \\ \dfrac{Z_V - X_{\mathrm{t}V}\sin\alpha_{\mathrm{e}}}{V - Z_{\dot{\alpha}}} & \dfrac{Z_\alpha}{V - Z_{\dot{\alpha}}} & \dfrac{-g\sin\mu_{\mathrm{e}}}{V - Z_{\dot{\alpha}}} & \dfrac{V + Z_q}{V - Z_{\dot{\alpha}}} \\ 0 & 0 & 0 & 1 \\ \dfrac{M_{\dot{\alpha}}(Z_V - X_{\mathrm{t}V}\sin\alpha_{\mathrm{e}})}{V - Z_{\dot{\alpha}}} + M_V + M_{\mathrm{t}V} & \dfrac{M_{\dot{\alpha}}Z_\alpha}{V - Z_{\dot{\alpha}}} + M_\alpha & \dfrac{-gM_{\dot{\alpha}}\sin\mu_{\mathrm{e}}}{V - Z_{\dot{\alpha}}} & \dfrac{M_{\dot{\alpha}}(V + Z_q)}{V - Z_{\dot{\alpha}}} + M_q \\ 0 & 0 & 0 & 0 \\ 0 & 0 & 0 & 0 \end{bmatrix} \cdot \begin{bmatrix} V_i \\ \alpha_i \\ \theta_i \\ q_i \\ \delta_{\mathrm{t}_i} \\ \delta_{\mathrm{e}_i} \end{bmatrix} + \begin{bmatrix} 0 & 0 \\ 0 & 0 \\ 0 & 0 \\ 0 & 0 \\ -\dfrac{1}{T_{\mathrm{t}}} & 0 \\ 0 & -\dfrac{1}{T_{\mathrm{e}}} \end{bmatrix} \cdot \begin{bmatrix} X_{\delta_{\mathrm{t}}}\cos\alpha_{\mathrm{e}} & X_{\delta_{\mathrm{e}}} \\ \dfrac{-X_{\delta_{\mathrm{t}}}\sin\alpha_{\mathrm{e}}}{V - Z_{\dot{\alpha}}} & \dfrac{Z_{\delta_{\mathrm{e}}}}{V - Z_{\dot{\alpha}}} \\ 0 & 0 \\ -\dfrac{M_{\dot{\alpha}}X_{\delta_{\mathrm{t}}}\sin\alpha_{\mathrm{e}}}{V - Z_{\dot{\alpha}}} + M_{\delta_{\mathrm{t}}} & \dfrac{M_{\dot{\alpha}}Z_{\delta_{\mathrm{e}}}}{V - Z_{\dot{\alpha}}} + M_{\delta_{\mathrm{e}}} \\ -\dfrac{1}{T_{\mathrm{t}}} & 0 \\ 0 & -\dfrac{1}{T_{\mathrm{e}}} \end{bmatrix} \begin{bmatrix} \delta_{\mathrm{t}_i,\mathrm{d}} \\ \delta_{\mathrm{e}_i,\mathrm{d}} \end{bmatrix}. \tag{8}
$$

$$
\begin{bmatrix} \dot{\beta}_i \\ \dot{\phi}_i \\ \dot{\psi}_i \\ \dot{p}_i \\ \dot{r}_i \\ \dot{\delta}_{\mathrm{a}_i} \\ \dot{\delta}_{\mathrm{r}_i} \end{bmatrix} = \begin{bmatrix} \dfrac{Y_\beta}{V} & \dfrac{g\cos\mu_{\mathrm{e}}}{V} & 0 & \dfrac{Y_p}{V} & \dfrac{Y_r - V}{V} & 0 & 0 \\ 0 & 0 & 0 & \dfrac{\cos\mu_{\mathrm{e}}}{\cos\theta_{\mathrm{e}}} & \dfrac{\sin\mu_{\mathrm{e}}}{\sin\theta_{\mathrm{e}}} & 0 & 0 \\ 0 & 0 & 0 & 0 & 1 & 0 & 0 \\ L^*_\beta & 0 & 0 & L^*_p & L^*_r & 0 & 0 \\ N^*_\beta & 0 & 0 & N^*_p & N^*_r & 0 & 0 \\ 0 & 0 & 0 & 0 & 0 & -\dfrac{1}{T_{\mathrm{a}}} & 0 \\ 0 & 0 & 0 & 0 & 0 & 0 & -\dfrac{1}{T_{\mathrm{r}}} \end{bmatrix} \begin{bmatrix} \beta_i \\ \phi_i \\ \psi_i \\ p_i \\ r_i \\ \delta_{\mathrm{a}_i} \\ \delta_{\mathrm{r}_i} \end{bmatrix} + \begin{bmatrix} \dfrac{Y_{\delta\mathrm{a}}}{V} & \dfrac{Y_{\delta\mathrm{r}}}{V} \\ 0 & 0 \\ 0 & 0 \\ L^*_{\delta\mathrm{a}} & L^*_{\delta\mathrm{r}} \\ N^*_{\delta\mathrm{a}} & N^*_{\delta\mathrm{r}} \\ -\dfrac{1}{T_{\mathrm{a}}} & 0 \\ 0 & -\dfrac{1}{T_{\mathrm{r}}} \end{bmatrix} \begin{bmatrix} \delta_{\mathrm{a}_i,\mathrm{d}} \\ \delta_{\mathrm{r}_i,\mathrm{d}} \end{bmatrix}. \tag{11}
$$

3.3 Stability analysis

Generally, providing the consistent criterion is very essential for a consensus algorithm. Afterward, the focus of this part is analyzing the closed-loop stability of the multi-UAV formation system with the cooperative guidance law (6) and the cooperative control law (19).

Using state equations and matrix analysis to obtain the necessary and sufficient condition, the theoretical deduction process for obtaining the consistent criteria is divided into five steps. Beginning from the cooperative control law (19), state equations of the whole formation will be given step by step. More precisely, it is necessary to deduce the close-loop state equations of a single UAV using the cooperative control law before computing state equations of the whole formation.

Then the process for obtaining the consistent criterion is given as follows:

1. For simplicity, Eq. (19) can be expressed in the observable canonical form, the detailed process of which can be found in Shi (2008):

$$
\begin{cases} \dot{\boldsymbol{x}}_i^{\mathrm{o}} = \boldsymbol{A}^{\mathrm{o}}\boldsymbol{x}_i^{\mathrm{o}} + \boldsymbol{B}^{\mathrm{o}}\boldsymbol{e}_{\bar{\boldsymbol{y}}_i}, \\ \boldsymbol{u}_i = \boldsymbol{C}^{\mathrm{o}}\boldsymbol{x}_i^{\mathrm{o}}, \end{cases} \tag{20}
$$

where $\boldsymbol{x}_i^{\mathrm{o}}$ are the state variables of the observable canonical form.

2. Compared with Eqs. (13) and (20), the cooperative control law (19) is united with the UAV model, obtaining state equations from $\boldsymbol{e}_{\bar{\boldsymbol{y}}_i}$ to $\bar{\boldsymbol{y}}_i$:

$$
\begin{cases} \dot{\boldsymbol{x}}_i^{\mathrm{e}} = \boldsymbol{A}^{\mathrm{e}}\boldsymbol{x}_i^{\mathrm{e}} + \boldsymbol{B}^{\mathrm{e}}\boldsymbol{e}_{\bar{\boldsymbol{y}}_i}, \\ \bar{\boldsymbol{y}}_i = \boldsymbol{C}^{\mathrm{e}}\boldsymbol{x}_i^{\mathrm{e}}, \end{cases} \tag{21}
$$

where $\boldsymbol{A}^{\mathrm{e}} = \left(\boldsymbol{I} - \begin{bmatrix} \boldsymbol{0} & \bar{\boldsymbol{B}}\boldsymbol{C}^{\mathrm{o}}\boldsymbol{A}^{\mathrm{o}} \\ \boldsymbol{0} & \boldsymbol{0} \end{bmatrix}\right)^{-1} \begin{bmatrix} \bar{\boldsymbol{A}} & \\ & \boldsymbol{A}^{\mathrm{o}} \end{bmatrix}$,

$\boldsymbol{B}^{\mathrm{e}}=\left(\boldsymbol{I}-\begin{bmatrix}\boldsymbol{0} & \bar{\boldsymbol{B}}\boldsymbol{C}^{\mathrm{o}}\boldsymbol{A}^{\mathrm{o}}\\ \boldsymbol{0} & \boldsymbol{0}\end{bmatrix}\right)^{-1}\begin{bmatrix}-\bar{\boldsymbol{B}}\boldsymbol{C}^{\mathrm{o}}(\boldsymbol{A}^{\mathrm{o}})^{-1}\boldsymbol{B}^{\mathrm{o}}\\ \boldsymbol{B}^{\mathrm{o}}\end{bmatrix}$, $\boldsymbol{C}^{\mathrm{e}}=[\bar{\boldsymbol{C}},\ \boldsymbol{0}]$, and $\boldsymbol{x}_i^{\mathrm{e}}=\left[[\bar{\boldsymbol{x}}_i]^{\mathrm{T}},\ [\boldsymbol{x}_i^{\mathrm{o}}]^{\mathrm{T}}\right]^{\mathrm{T}}$ are the state variables.

3. There exists $\dot{\boldsymbol{e}}_{\bar{\boldsymbol{y}}i}=\dot{\bar{\boldsymbol{y}}}_i-\boldsymbol{v}_i$, and the closed-loop state equations for a single UAV are obtained as

$$\begin{cases}\dot{\boldsymbol{x}}_i^{\mathrm{a}}=\boldsymbol{A}^{\mathrm{a}}\boldsymbol{x}_i^{\mathrm{a}}+\boldsymbol{B}^{\mathrm{a}}\boldsymbol{v}_i,\\ \bar{\boldsymbol{y}}_i=\boldsymbol{C}^{\mathrm{a}}\boldsymbol{x}_i^{\mathrm{a}},\end{cases}\tag{22}$$

where $\boldsymbol{A}^{\mathrm{a}}=\begin{bmatrix}\boldsymbol{0} & \boldsymbol{I}\\ \boldsymbol{0} & \bar{\boldsymbol{A}}+\bar{\boldsymbol{B}}\bar{\boldsymbol{C}}\end{bmatrix}$ is the state matrix, $\boldsymbol{B}^{\mathrm{a}}=\begin{bmatrix}\boldsymbol{0}\\ -\boldsymbol{B}^{\mathrm{e}}\end{bmatrix}$ is the input matrix, $\boldsymbol{C}^{\mathrm{a}}=[\boldsymbol{C}^{\mathrm{e}},\ \boldsymbol{0}]$ is the output matrix, $\boldsymbol{x}_i^{\mathrm{a}}=\left[[\boldsymbol{x}_i^{\mathrm{e}}]^{\mathrm{T}},\ [\dot{\boldsymbol{x}}_i^{\mathrm{e}}]^{\mathrm{T}}\right]^{\mathrm{T}}$ are the state variables, and the input $\boldsymbol{v}_i$ is the cooperative order defined in Eq. (6).

4. The state equations of the whole formation are given by

$$\begin{cases}\dot{\boldsymbol{x}}^{\mathrm{all}}=\boldsymbol{A}^{\mathrm{all}}\boldsymbol{x}^{\mathrm{all}}+\boldsymbol{B}^{\mathrm{all}}\boldsymbol{u}^{\mathrm{all}},\\ \boldsymbol{y}^{\mathrm{all}}=\boldsymbol{C}^{\mathrm{all}}\boldsymbol{x}^{\mathrm{all}},\end{cases}\tag{23}$$

where $\boldsymbol{x}^{\mathrm{all}}=\left[[\boldsymbol{x}_1^{\mathrm{a}}]^{\mathrm{T}},[\boldsymbol{x}_2^{\mathrm{a}}]^{\mathrm{T}},\dots,[\boldsymbol{x}_n^{\mathrm{a}}]^{\mathrm{T}}\right]^{\mathrm{T}}$, $\boldsymbol{y}^{\mathrm{all}}=[\bar{\boldsymbol{y}}_1,\bar{\boldsymbol{y}}_2,\dots,\bar{\boldsymbol{y}}_n]^{\mathrm{T}}$, $\boldsymbol{u}^{\mathrm{all}}=[\boldsymbol{v}_1,\boldsymbol{v}_2,\dots,\boldsymbol{v}_n]^{\mathrm{T}}$, $\boldsymbol{A}^{\mathrm{all}}=\mathrm{diag}(\boldsymbol{A}^{\mathrm{a}})_n$, $\boldsymbol{B}^{\mathrm{all}}=\mathrm{diag}(\boldsymbol{B}^{\mathrm{a}})_n$, and $\boldsymbol{C}^{\mathrm{all}}=\mathrm{diag}(\boldsymbol{C}^{\mathrm{a}})_n$.

5. As $\boldsymbol{v}_i=[\dot{V}_i^{\mathrm{g}},\dot{\theta}_i^{\mathrm{g}},\dot{\psi}_i^{\mathrm{g}}]^{\mathrm{T}}$ in the cooperative guidance law (6), nonlinear Eqs. (3)–(5) are small linearized disturbances:

$$\boldsymbol{v}_i=\boldsymbol{H}^{\mathrm{a}}\dot{\boldsymbol{V}}_i^{\mathrm{g}}.\tag{24}$$

According to Eqs. (3)–(5), matrix $\boldsymbol{H}^{\mathrm{a}}$ can be deduced. Define $\dot{\boldsymbol{V}}^{\mathrm{gall}}=\left[[\dot{\boldsymbol{V}}_1^{\mathrm{g}}]^{\mathrm{T}},[\dot{\boldsymbol{V}}_2^{\mathrm{g}}]^{\mathrm{T}},\dots,[\dot{\boldsymbol{V}}_n^{\mathrm{g}}]^{\mathrm{T}}\right]^{\mathrm{T}}$ and $\boldsymbol{H}^{\mathrm{all}}=\mathrm{diag}(\boldsymbol{H}^{\mathrm{a}})_n$, and then substitute Eq. (24) into Eq. (23) to obtain

$$\begin{cases}\dot{\boldsymbol{x}}^{\mathrm{all}}=\boldsymbol{A}^{\mathrm{all}}\boldsymbol{x}^{\mathrm{all}}+\boldsymbol{B}^{\mathrm{all}}\boldsymbol{H}^{\mathrm{all}}\dot{\boldsymbol{V}}^{\mathrm{gall}},\\ \boldsymbol{y}^{\mathrm{all}}=\boldsymbol{C}^{\mathrm{all}}\boldsymbol{x}^{\mathrm{all}}.\end{cases}\tag{25}$$

There exists $\dot{\boldsymbol{V}}^{\mathrm{gall}}=-(\boldsymbol{\Gamma}\otimes\boldsymbol{I}_3)\boldsymbol{y}^{\mathrm{all}}$ such that Eq. (23) can be transformed into a linear time-invariant system, where '$\otimes$' represents the Kronecker product and $\boldsymbol{\Gamma}$ is the expanded matrix of the communication topology (Shi, 2008):

$$\begin{aligned}\dot{\boldsymbol{x}}^{\mathrm{all}}&=\boldsymbol{A}^{\mathrm{all}}\boldsymbol{x}^{\mathrm{all}}+\boldsymbol{B}^{\mathrm{all}}\boldsymbol{H}^{\mathrm{all}}\left(-(\boldsymbol{\Gamma}\otimes\boldsymbol{I}_3)\boldsymbol{y}^{\mathrm{all}}\right)\\ &=\boldsymbol{A}^{\mathrm{all}}\boldsymbol{x}^{\mathrm{all}}+\boldsymbol{B}^{\mathrm{all}}\boldsymbol{H}^{\mathrm{all}}\left(-(\boldsymbol{\Gamma}\otimes\boldsymbol{I}_3)\boldsymbol{C}^{\mathrm{all}}\boldsymbol{x}^{\mathrm{all}}\right)\\ &=\left(\boldsymbol{A}^{\mathrm{all}}-\boldsymbol{B}^{\mathrm{all}}\boldsymbol{H}^{\mathrm{all}}(\boldsymbol{\Gamma}\otimes\boldsymbol{I}_3)\boldsymbol{C}^{\mathrm{all}}\right)\boldsymbol{x}^{\mathrm{all}}.\end{aligned}\tag{26}$$

Until now, the state equations Eq. (25) come to a linear time-invariant system without control input, which is caused by the initial condition. It is possible to analyze whether system (26) is stable or not. If and only if all non-zero eigenvalues of $(\boldsymbol{A}^{\mathrm{all}}-\boldsymbol{B}^{\mathrm{all}}\boldsymbol{H}^{\mathrm{all}}(\boldsymbol{\Gamma}\otimes\boldsymbol{I}_3)\boldsymbol{C}^{\mathrm{all}})$ have negative real parts, system (26) is stable, which is a necessary and sufficient condition for the multi-UAV formation system with the cooperative guidance law (6) and the cooperative control law (19).

3.4 Synchronization technology

Measurement errors always exist in practice, which is harmful to formation control and will decrease the stability and accuracy. Under the influence of navigation and range finding, position data contain measurement errors:

$$\begin{cases}x_i^*=x_i+\tilde{x}_i,\\ y_i^*=y_i+\tilde{y}_i,\\ z_i^*=z_i+\tilde{z}_i,\end{cases}\tag{27}$$

where $\tilde{x}_i$, $\tilde{y}_i$, and $\tilde{z}_i$ are the measurement errors. Therefore, the measurement values x_i^* , y_i^*, and z_i^* are used to replace the real values x_i, y_i, and z_i, respectively. Define $\boldsymbol{\rho}_{i\mathrm{F}}^*=(x_{i\mathrm{F}}^*,y_{i\mathrm{F}}^*,z_{i\mathrm{F}}^*)^{\mathrm{T}}$ as new position coordination variables:

$$\boldsymbol{\rho}_{i\mathrm{F}}^*=\boldsymbol{\rho}_i^*+\boldsymbol{\rho}_{i\mathrm{F}}^{\mathrm{d}}.\tag{28}$$

Substitute Eq. (28) into Eq. (2) to obtain the acceleration for cooperative guidance:

$$\begin{cases}\dot{V}_{x_i}^{\mathrm{g}}=-\sum\limits_{j\in\mathcal{N}_i}a_{ij}[x_{i\mathrm{F}}^*-x_{j\mathrm{F}}^*-\gamma\dot{x}_{ij}^*],\\ \dot{V}_{y_i}^{\mathrm{g}}=-\sum\limits_{j\in\mathcal{N}_i}a_{ij}[y_{i\mathrm{F}}^*-y_{j\mathrm{F}}^*-\gamma\dot{y}_{ij}^*],\\ \dot{V}_{z_i}^{\mathrm{g}}=-\sum\limits_{j\in\mathcal{N}_i}a_{ij}[z_{i\mathrm{F}}^*-z_{j\mathrm{F}}^*-\gamma\dot{z}_{ij}^*].\end{cases}\tag{29}$$

To overcome the flaw, the synchronization technology is proposed, which works in an effective and efficient way because the technology uses the cross-coupling concept to synchronize the relative position tracking motion of the aircraft. For simplicity, the channel x is chosen to improve the control accuracy. It uses synchronization error:

$$e_{x_i}=-\sum_{j\in\mathcal{N}_i}a_{ij}\left[(x_{i\mathrm{F}}^*-x_{j\mathrm{F}}^*)+c_i(\dot{x}_{i\mathrm{F}}^*-\dot{x}_{j\mathrm{F}}^*)\right],\tag{30}$$

which incorporates error information from different UAVs in the system to identify the performance of

synchronization. In Eq. (30), c_i is a positive constant less than 1. The cross-coupled error $e^*_{x_i}$ then couples the measurement error $\tilde{x}_i$ and synchronization error e_{x_i} through a positive synchronization gain d_{x_i}:

$$e^*_{x_i} = \tilde{x}_i + d_{x_i} e_{x_i}. \tag{31}$$

The objective of the synchronization strategy is to drive $e^*_{x_i}$ of each UAV in Eq. (31) to zero asymptotically by choosing proper gain values, implying that both $\tilde{x}_i$ and e_{x_i} are driven to zero as well. Likewise, the cross-coupled errors $e^*_{y_i}$ and $e^*_{z_i}$ for y and z channels are defined in the same way. Then let $\boldsymbol{e}^*_{x_i} = [e^*_{x_i}, e^*_{y_i}, e^*_{z_i}]^{\mathrm{T}}$, to calculate the modification $\Delta\dot{\boldsymbol{V}}_i^{\mathrm{g}*}$. The new modified trajectory command will be passed to Eq. (2). The new cooperative control law is $\dot{\boldsymbol{V}}_i^{\mathrm{g}*} = \dot{\boldsymbol{V}}_i^{\mathrm{g}} + \Delta\dot{\boldsymbol{V}}_i^{\mathrm{g}*}$, where $\Delta\dot{\boldsymbol{V}}_i^{\mathrm{g}*}$ is the synchronization technology given by the state feedback:

$$\Delta\dot{\boldsymbol{V}}_i^{\mathrm{g}*} = \boldsymbol{K}_3 \boldsymbol{e}^*_i + \boldsymbol{K}_4 \int_0^t \boldsymbol{e}^*_i \mathrm{d}t, \tag{32}$$

in which $\boldsymbol{K}_3$ and $\boldsymbol{K}_4$ are feedback gains of the synchronization technology, selected using the pole placement method (Liu and Tang, 2000).

4 Numerical simulation

Using the six-degree-of-freedom dynamic UAV model (Eq. (13)), the multi-UAV formation control strategy is simulated with five aircrafts, where all UAVs are considered identical. The performance of the whole formation will be analyzed, where no collision avoidance algorithm is implemented. Each UAV weighs 85 kg with a wingspan of 2.4 m. Fig. 4 shows the communication network. An edge from U_j to U_i means that U_i can receive information from U_j.

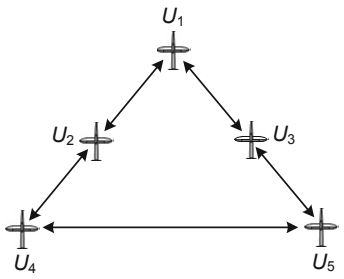

Fig. 4 Communication topology

All the UAVs have to maintain an equilateral triangular formation, with side length of 8 m. Besides, they do not fly at an identical altitude. Rather, U_2 and U_3 maneuver 4 m lower than U_1, while U_4 and U_5 are 8 m lower than U_1. However, the team does not start at the desired positions in the beginning.

The simulation time is 200 s, and each operation step takes 0.02 s. Simulations are performed for the cooperative guidance law (6) and the cooperative control law (19), where the synchronization technology (32) is also validated. The maximum velocity of the formation is 46 m/s and the minimum is 32 m/s. Other initial parameters of each UAV are given in Table 1.

Table 1 Initial parameters of each unmanned aerial vehicle

UAV	$\boldsymbol{\rho}(t_0)$ (m)	$V(t_0)$ (m/s)	$\theta(t_0)$ (°)	$\psi(t_0)$ (°)
U_1	$[20, 5, 502]^{\mathrm{T}}$	38.0	−2.3	48.8
U_2	$[10, 10, 496]^{\mathrm{T}}$	39.0	0	57.4
U_3	$[30, -5, 494]^{\mathrm{T}}$	40.8	3.8	68.5
U_4	$[10, 5, 492]^{\mathrm{T}}$	39.0	2.0	62.8
U_5	$[20, -10, 490]^{\mathrm{T}}$	40.0	−1.2	53.0

There is white Gaussian noise in the measurement of position, with mean value of 0 m and variance of 1 m^2 in the x, y, z channels. Formation synchronization errors are defined as Eq. (30) with $c = 0.2$. The synchronization gains $d_{x_i}, d_{y_i}, d_{z_i}$ in the synchronization technology (32) for these vehicles are all set to 0.3.

Applying the cooperative guidance law (6), the cooperative control law (19), and the suggested synchronization technology (32), Fig. 5 illustrates the position and attitude of the team, Fig. 6 depicts the cross-coupled errors, and Fig. 7 shows the comparison of both methods with and without synchronization technology (32).

Fig. 5 shows the velocity, pitch, heading, and the three-dimensional position. The trajectory of the team is represented clearly in Fig. 5d. Fig. 5e shows the three-dimensional position after stabilization in a short time, which is the last part of Fig. 5d. Only the last six sampling points are adopted within 0.1 s. It can be seen that position and attitude of the team do not satisfy the desired request in the beginning. Under the influence of the cooperative guidance law (6) and the cooperative control law (19), both position and attitude achieve consensus and the team stabilizes within 100 s; afterward, these UAVs maintain good triangular configuration.

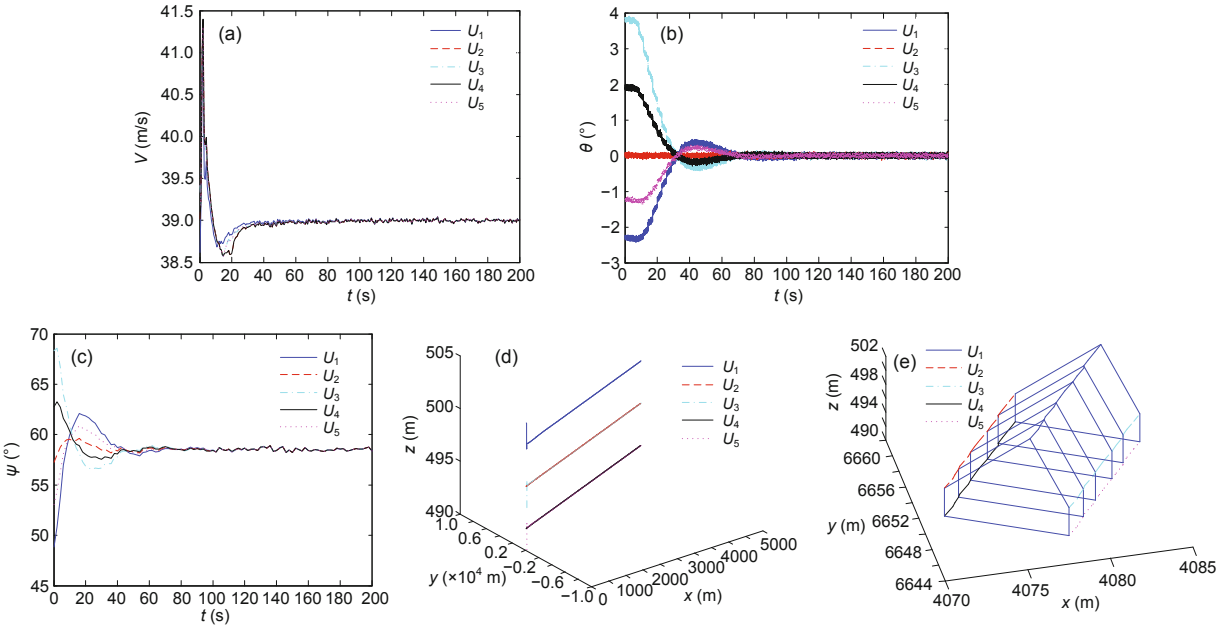

Fig. 5 Position and attitude of the formation: (a) velocity; (b) pitch; (c) heading; (d) three-dimensional position; (e) local three-dimensional position

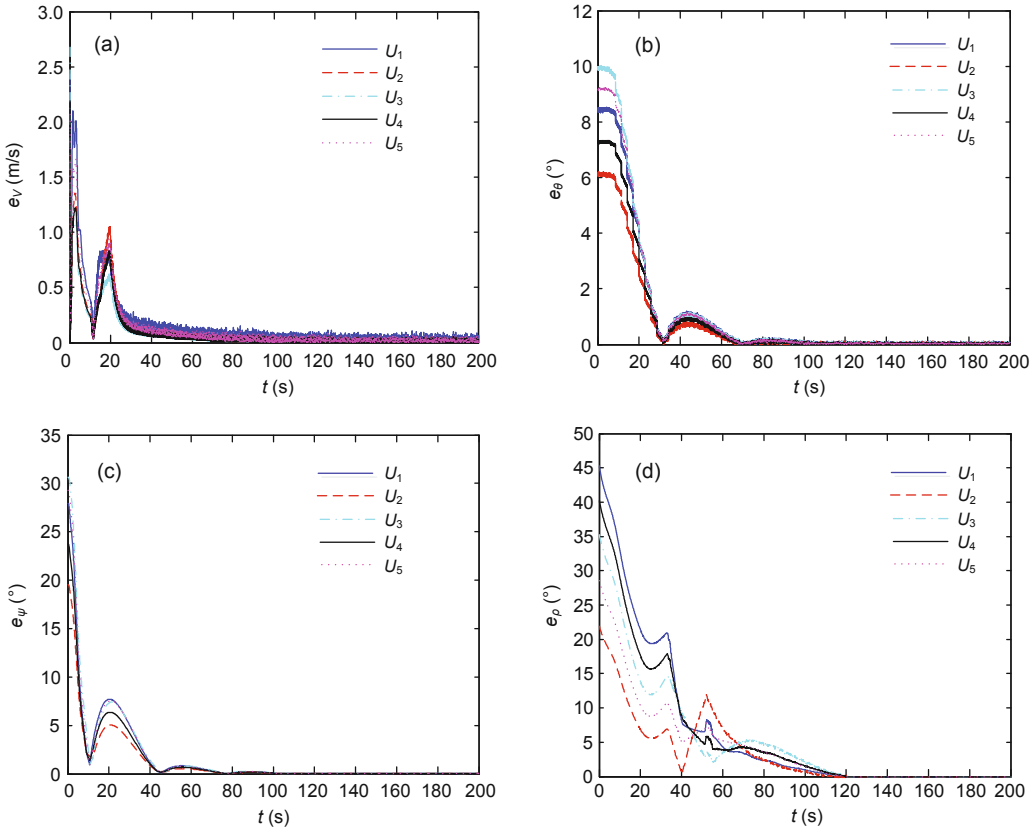

Fig. 6 Cross-coupled errors of the formation: (a) velocity errors; (b) pitch errors; (c) heading errors; (d) three-dimensional position errors

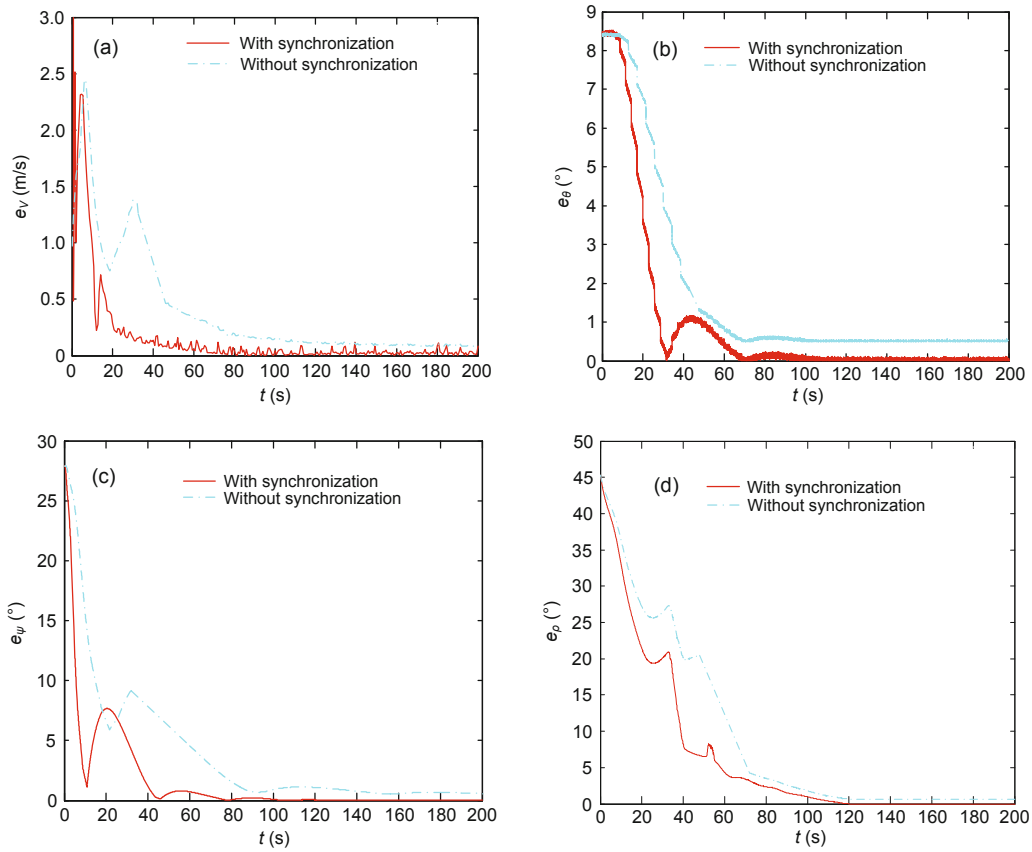

Fig. 7 Cross-coupled errors of the formation with and without synchronization technology: (a) velocity errors; (b) pitch errors; (c) heading errors; (d) three-dimensional position errors

Fig. 6 shows errors of velocity, pitch, heading, and the three-dimensional position. Though there is noise in the measurement of position, the errors decrease and approach zero asymptotically within 100 s, which is in agreement with the position and attitude curves in Fig. 5. Specifically, three-dimensional position errors, which approach zero after 100 s in Fig. 6d, clearly show that the formation shape is kept well. In a word, these curves of errors also validate the effectiveness of the cooperative guidance law (6) and the cooperative control law (19).

To compare the two methods with and without synchronization technology (32), only the error curves of U_1 are chosen as representatives. In Fig. 7, the errors of velocity, pitch, heading, and the three-dimensional position for these two methods are shown together. In comparison, though both methods can stabilize the formation, the effect of depressing measurement errors and synchronization errors with synchronization technology (32) is better, with smaller steady-state error and faster decreasing speed. Therefore, it is validated that synchronization technology (32) is good at depressing errors and improving control accuracy.

5 Conclusions

In this paper, we considered a multi-UAV formation control strategy based on second-order consensus. A cooperative guidance algorithm and a cooperative control algorithm were designed together to maintain a specified geometric configuration. The cooperative guidance law is a second-order consensus algorithm, providing the desired acceleration, pitch rate, and heading rate. The cooperative control law is easy to construct by choosing proper feedback gains. By theoretically analyzing the closed-loop stability of the formation system and dividing the deducing process into five steps, the necessary

and sufficient condition of closed-loop stability was obtained, which is that the formation system is stable if and only if all non-zero eigenvalues of the formation system have negative real parts. Three-dimensional formation flight simulation shows that, by using the synchronization technology, both measurement errors and synchronization errors were driven to zero asymptotically. Control effort of each UAV has quick response and high control precision, which makes the proposed multi-UAV formation control strategy a good candidate for engineering applications.

References

Aldo, S., Jaimes, B., Jamshidi, M., 2010. Consensus-based and network control of UAVs. Proc. 5th Int. Conf. on System of Systems Engineering, p.1-6. http://dx.doi.org/10.1109/SYSOSE.2010.5544106

Annamalai, A., Motwani, A., Sharma, S.K., *et al.*, 2015. A robust navigation technique for integration in the guidance and control of an uninhabited surface vehicle. *J. Navigat.*, **68**(4):750-768. http://dx.doi.org/10.1017/S0373463315000065

Bai, C., Duan, H., Li, C., *et al.*, 2009. Dynamic multi-UAVs formation reconfiguration based on hybrid diversity-PSO and time optimal control. Proc. IEEE Intelligent Vehicles Symp., p.775-779. http://dx.doi.org/10.1109/IVS.2009.5164376

Bennet, D.J., McInnes, C.R., Suzuki, M., *et al.*, 2011. Autonomous three-dimensional formation flight for a swarm of unmanned aerial vehicles. *J. Guid. Contr. Dynam.*, **34**(6):1899-1908. http://dx.doi.org/10.2514/1.53931

Chen, X., Zhang, C., 2013. The method of multi unmanned aerial vehicle cooperative tracking in formation based on the theory of consensus. Proc. 5th Int. Conf. on Intelligent Human-Machine Systems and Cybernetics, p.148-151. http://dx.doi.org/10.1109/IHMSC.2013.182

Fukushima, H., Kon, K., Matsuno, F., 2013. Model predictive formation control using branch-and-bound compatible with collision avoidance problems. *IEEE Trans. Robot.*, **29**(5):1308-1317. http://dx.doi.org/10.1109/TRO.2013.2262751

Hou, H., Wei, R.X., Liu, Y., *et al.*, 2011. UAV control method studied based on high-order sliding mode control. *Flight Dynam.*, **29**(1):38-41 (in Chinese). http://dx.doi.org/10.13645/j.cnki.f.d.2011.01.010

Jing, Y., Shi, X.P., 2014. NDI formation controller design for UAV based on super twisting algorithm. *J. Syst. Eng. Electron.*, **36**(7):1380-1385 (in Chinese). http://dx.doi.org/10.3969/j.issn.1001-506X.2014.07.24

Kim, S., Kim, Y., 2007. Three dimensional optimum controller for multiple UAV formation flight using behavior-based decentralized approach. Proc. Int. Conf. on Control, Automation and Systems, p.1387-1392. http://dx.doi.org/10.1109/ICCAS.2007.4406555

Kumar, R., Kabamba, P., Hyland, D.C., 2005. Controller design using adaptive random search for close-coupled formation flight. *J. Guid. Contr. Dynam.*, **28**(6):1323-1326. http://dx.doi.org/10.2514/1.11377

Kuriki, Y., Namerikawa, T., 2013. Consensus-based cooperative control for geometric configuration of UAVs flying in formation. Proc. SICE Annual Conf., p.1237-1242.

Kuriki, Y., Namerikawa, T., 2014. Consensus-based cooperative formation control with collision avoidance for a multi-UAV system. Proc. American Control Conf., p.2077-2082. http://dx.doi.org/10.1109/ACC.2014.6858777

Li, S., Chen, Y., Yang, Z., *et al.*, 2012. Formation fight control of multi-UAVs with communication delay. *Inform. Contr.*, **41**(2):142-146 (in Chinese). http://dx.doi.org/10.3724/SP.J.1219.2012.00142

Liu, B., Tang, W., 2000. Modern Control Theory. China Machine Press, Beijing, p.193-199 (in Chinese).

Mercado, D.A., Castro, R., Lozano, R., 2013. Quadrotors flight formation control using a leader-follower approach. Proc. European Control Conf., p.3858-3863.

Ren, W., 2006. Consensus based formation control strategies for multi-vehicle systems. Proc. American Control Conf., p.4237-4242. http://dx.doi.org/10.1109/ACC.2006.1657384

Ren, W., Beard, R., 2002. Virtual structure based spacecraft formation control with formation feedback. Proc. AIAA Guidance, Navigation, and Control Conf. and Exhibit, p.1-8. http://dx.doi.org/10.2514/6.2002-4963

Seo, J., Ahn, C., Kim, Y., 2009. Controller design for UAV formation flight using consensus based decentralized approach. Proc. AIAA Infotech@Aerospace Conf., p.1-11. http://dx.doi.org/10.2514/6.2009-1826

Shan, J., Liu, H., 2005. Close-formation flight control with motion synchronization. *J. Guid. Contr. Dynam.*, **28**(6):1316-1320. http://dx.doi.org/10.2514/1.13953

Shi, Z.K., 2008. Linear System Theory. Science Press, Beijing (in Chinese).

Wang, J., Wei, R., Dong, Z., *et al.*, 2010. Research on formation flight control of cooperative UAV. *Fire Contr. Command Contr.*, **35**(3):34-38.

Wang, X.Y., Wang, X.M., Xiao, Y.H., *et al.*, 2012. Design of robust H_∞ controller for UAVs three-dimensional formation flight. *Contr. Dec.*, **27**(12):1907-1911 (in Chinese). http://dx.doi.org/10.13195/j.cd.2012.12.150.wangxy.004

Xiao, Y.H., Wang, X.M., Wang, X.Y., 2011. An effective controller design of formation flight of unmanned aerial vehicles (UAV). *J. Northwestern Polytech. Univ.*, **29**(6):834-838 (in Chinese).